Cyclic Oxidation Modeling and Life Prediction

James L. Smialek
NASA Glenn Research Center, 21000 Brookpark Rd., Cleveland, OH 44135 USA
James.L.Smialek@NASA.gov

Keywords: cyclic oxidation, modeling, scale growth, spallation, alumina scales.

Abstract. The cyclic oxidation process can be described as an iterative scale growth and spallation sequence by a number of similar models. Model input variables include oxide scale type and growth parameters, spalling geometry, spall constant, and cycle duration. Outputs include net weight change, the amounts of retained and spalled oxide, the total oxygen and metal consumed, and the terminal rates of weight loss and metal consumption. All models and their variations produce a number of similar characteristic features. In general, spalling and material consumption increase to a steady state rate, at which point the retained scale approaches a constant and the rate of weight loss becomes linear. For one model, this regularity was demonstrated as dimensionless, universal expressions, obtained by normalizing the variables by critical performance factors. These insights were enabled through the use of the COSP for Windows cyclic oxidation spalling program.

Introduction

For isothermal exposures, degradation from oxidation is easily defined on the basis of scale growth models alone. However, in cyclic exposures, protective scales may be especially compromised because some portion of the scale may spall off on cooldown due to extremely high compressive thermal expansion misfit stresses. The primary effect is that, after portions of the scale are removed, re-growth of a thinner scale occurs at rates higher than those for continued growth of the undamaged thicker scale. This spalling amount and configuration is therefore just as important as growth rate in determining metal consumption. Rather than fit experimental weight change curves, the purpose of this paper is to highlight and review the typical trends predicted for oxidation and metal consumption as a function of oxide type, growth kinetics, spalling formalisms, and cycle duration. Universal response curves for one particular model are presented by using dimensionless, normalized parameters.

Elements of Cyclic Oxidation Models

Various models have been put forth to describe these processes and successfully fit experimental cyclic oxidation curves to model predictions [1-3]. Perhaps the most all-inclusive treatise is the COSP Cyclic Oxidation Spalling Program [2-4]. This model applies to the majority of the topics discussed below, except where specifically noted.

Scale Growth Models. Scale growth is normally characterized in isothermal tests, and parabolic rates are normally encountered for protective scales due to diffusion control of the growth process. Modifications due to scale grain growth coupled with grain boundary diffusion control or due to rapid transient oxidation occurring before protective healing layers are formed may lead to power law or logarithmic rates as listed below [2]:

$$\text{parabolic:} \quad (\Delta W/A)^2 = (k_p t) \tag{1}$$

$$\text{power law:} \quad (\Delta W/A)^m = (kt) \tag{2}$$

$$\text{logarithmic} \quad (\Delta W/A) = \ln [(kt+c)^{1/m}] \tag{3}$$

Spalling Models. The geometry or "fractopography' of the spalled portion must be specified in order to completely define the thickness of the retained scale and the corresponding growth rate upon reheating. At one extreme, all spallation is assumed to occur uniformly as an outer layer of the scale, Figure 1, Case A. This would apply to extremely adherent scales that remain attached to the substrate, then fracture *within* the scale after accumulating a sufficient amount of stored strain energy. While a single uniform layer is not observed in practice, it represents a simplifying assumption and approximates the response, on average, over the entire sample surface.

At the other extreme is the use of discrete segments which *do* spall completely to the scale-metal interface, Fig. 1, Case C. And an intermediate situation, Case B, allows for segment spallation at some depth fraction of the scale thickness, R_s. Finally a bimodal combination of A and B (or C), each having different depth fractions of spallation, R_s, and each with a representative spalling probability, P_1 and P_2, is proposed. For these configurations, rather than picking the same segments to spall on every cycle, the occurrence is randomized over all segments by means of a Monte Carlo algorithm [2].

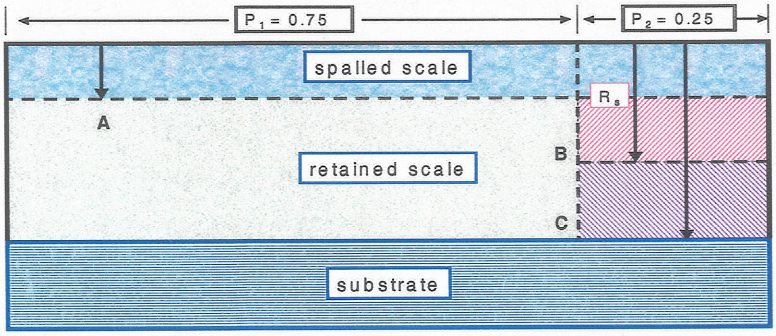

Figure 1. Various schemes of scale 'fractopography' for COSP models.
A) uniform surface layer;
B) partial depth fraction, R_s;
C) full interfacial segment;
A + (B or C) bimodal, with probabilities of P_1 and P_2.

Spalling Formalisms. One of the earliest models employed a constant interfacial spalling area fraction, k_s, wherein each successive cycle caused every segment to spall 'k_s' of its area, leaving an unspalled area fraction equal to $(1-k_s)$ [1]. This model required the unusual morphology of having 2^i segments, where i refers to number of cycles, resulting in a relative area of $(1-k_s)^i$ of originally intact oxide. A more recent interfacial model, DICOSM, (Deterministic Interfacial Cyclic Oxidation Spalling Program), also specifies a constant area fraction, F_A, to spall at the interface, but only at the thickest portion of the scale [5]. But here the number of effective area segments is now fixed, as $1/F_A$. A similar interfacial model has defined the spalling process by a statistical probability factor, p, which relates the overall tendency for the scale to spall on any given cycle [6,7]. Identical behavior is observed between the probabilistic, p, and the area fraction interfacial model, k_s, but divergence occurs between these and the DICOSM, F_A, interfacial model.

A more general formalism, described by COSP for any of its configurations, defines the mass spalling fraction, F_s, as a function of the mass of oxide present before cooldown, W_r':

$$F_s = Q_o W'_r{}^{\alpha} \qquad (4)$$

where Q_o is a constant and the spall exponent α, usually fixed at 1.0, reflects the spalling dependence on scale thickness suggested by independent experiments [2]. Note that for the special case of $\alpha = 0$, the spall fraction F_s is a constant.

The general sequence of the algorithm is that the scale is grown for a cycle duration of Δt, and a portion is allowed to spall according to eq. 4 above. The amount of retained scale is calculated and the growth upon the next cycle must be determined. For the latter, COSP uses the concept of effective time, t_{eff}, which is equivalent to that needed to grow the retained mass of scale in an isothermal exposure. Thus the total amount of new scale follows from the growth law selected from eq's. 1-3, when $t_{eff} + \Delta t$ is now substituted for the time, t.

The inputs, as called for in the publicly available software, COSP for Windows [4], thus require choosing a growth model and spalling configuration and specification of growth constants (k, m, and c), cycle duration (Δt), oxide phase or the stoichiometric constant (S_c = mass oxide/mass oxygen in oxide), spall constants (Q_o) or area fraction (F_A), and spall exponent (α). For the Monte Carlo option, spall depth fraction (R_{spall}) and number of segments (n) are also required. Interfacial spallation is therefore handled by using an R_{spall}=1.0. The primary output is the net sample weight (mass) change ($\Delta W/A$) per cycle, but also includes the total amount of oxygen and metal reacted (ΣW_{ox}, ΣW_m), the current amount of retained scale (W_r) and the total amount and current fraction of scale spalled (ΣW_s, F_s). No mechanistic assumptions are required (critical values of oxide thickness, strain energy, sulfur content, aluminum content, etc.).

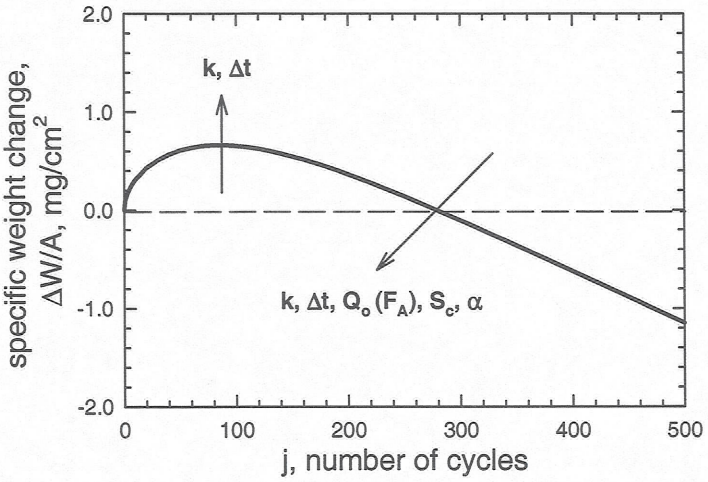

Figure 2. Trends with input parameters for COSP cyclic oxidation weight change curve [8]. Example shown for parabolic growth, uniform layer spalling for Al_2O_3: k_p = 0.01 mg^2/cm^{4}hr, Δt = 1 hr, Q_o = 0.002 cm^2/mg, m = 2.0, α = 1.0.

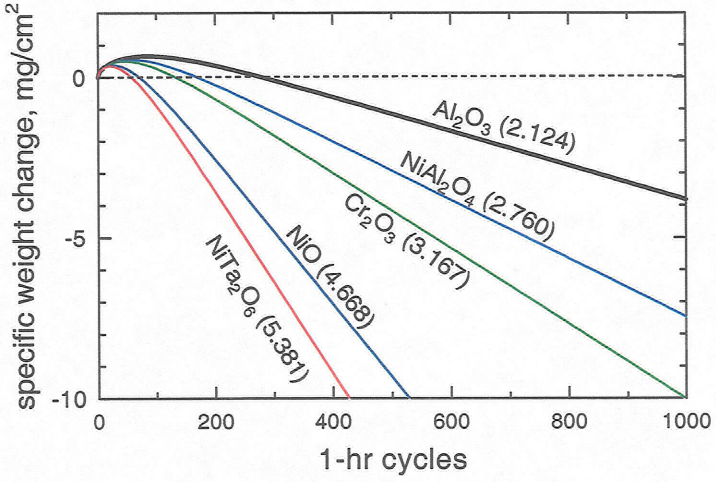

Figure 3. The effect of oxide type (S_c) on model cyclic oxidation curves [4]. Uniform layer spallation: (k_p= 0.01mg^2/cm^4/hr, Q_o= 0.002 cm^2/mg, Δt=1 hr).

Cyclic Oxidation Responses.

A typical model weight change vs number of cycles curve, Fig. 2, exhibits features similar to experimental curves: a maximum in the weight change, followed by a decrease to zero weight change and a final linear rate of loss. Regular trends in this and other outputs have been described in more detail previously in [1-5] and are suggested by the arrows. The maximum increases with the growth factor $k_p\Delta t$, but decreases with metal content in the scale S_c and spall constant Q_o (or generally increased by all these parameters. The number of cycles to reach maximum (j_{max}) and cross zero (j_o) are decreased by all these parameters for cases where the COSP spall exponent α>0, but remains invariant with $k_p\Delta t$ for the constant area fraction models [1,5], for the fixed probability models [6,7], and for COSP cases with α=0. It is found that the ratio of j_o/j_{max} is exactly 3.0 for most DICOSM cases and approaches 3.3 for the COSP uniform layer model (for Al_2O_3 and α=1), thus in a sense determining the general form of the weight change curve.

The actual response for various common oxides are shown in Fig. 3. Because the metal mass content increases with S_c by definition, the effect on spalling is manifested here as higher rates of weight loss, even for the same growth rate, as in Fig.3.

A more subtle effect is the decrease in the j_o/j_{max} ratio, thus changing the ideal form of the curve as well. In fact, for the most general COSP models, it can be shown that this j_o/j_{max} ratio, or shape index, is not really a constant at all. This effect is more explicitly presented in Fig. 4, showing significant decreases in the index with increasing stoichiometric mass factors, S_c. Furthermore, it is seen that the growth exponent (linear, parabolic, or cubic with m=1, 2, or 3 in eqn.1) greatly increases the shape index. Finally, the spalling exponent, α, also has an effect.

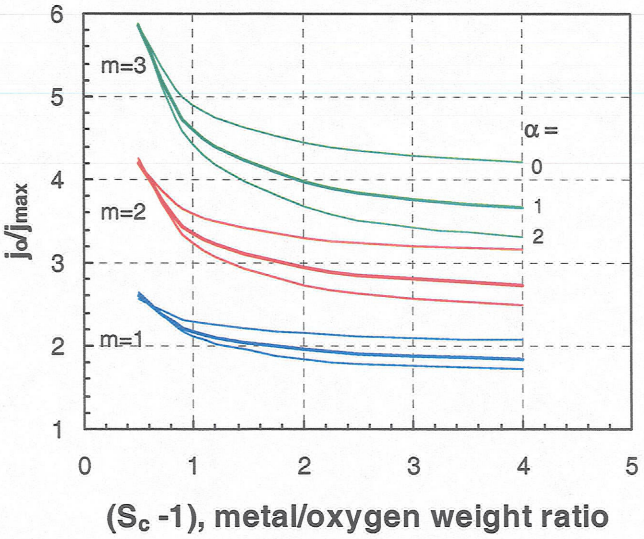

Figure 4. Variations in shape factor of COSP model weight change curves: decreases with stoichiometric factor, S_c; increases with growth exponent (m=1,2,3) for linear, parabolic, cubic kinetics; and decreases with spall exponents, α=1,2, 3.

Thus low metal content scales, growing with sub-parabolic kinetics, and with a constant spall fraction can be expected to exhibit the highest shape index and a cyclic weight maximum greatly skewed towards the origin. To illustrate the shape factor for the most popular case, it can be seen that an S_c of 2.124 for Al_2O_3, with parabolic growth and a spalling exponent of 1, indeed produces a shape factor of 3.27 as discussed above. While these basic variations may be disconcerting to a cyclic oxidation modeling effort, it is noted that the shape factor is nevertheless invariant with a number of other model parameters such as k, Δt, or Q_o.

Other outputs. The models also calculate various other elements germane to the cyclic process. The total amount of oxygen reacted, aluminum consumed, and oxide spalled are shown for the case of uniform spallation of an Al_2O_3 scale in Fig. 5. They can be seen to reach linear steady state rates of increase at essentially the point where the weight change curve crosses zero. Also shown is the weight of the retained scale after spallation (W_r) and the fractional amount of spalling (F_s). These reach essentially constant values as part of the steady state regime.

Comparison of various spalling conditions. From a systematic study of the various spalling formalisms over a range of input parameters, it is generally observed that the COSP uniform layer spalling model produces the least severe metal consumption rate for equivalent spall constants (Q_o) or with equivalent spall fractions (F_s). The DICOSM model can be most directly compared to COSP models where the value of the spall exponent $\alpha = 0$, i.e., the spall fraction is a constant, eq. 4. Here, for example, it is found that the terminal steady state rate of metal consumption for the COSP uniform layer spalling is about 20% less than the interfacial bimodal spalling (Monte Carlo) case and about 15% less than the interfacial DICOSM case. For DICOSM and these special COSP cases, i.e., where $\alpha = 0$, it is also found that the number of cycles to reach maximum and zero weight change do not vary with the input growth parameters (k_p, Δt). Basically, the curves are amplified vertically without changing the basic shape [2-5].

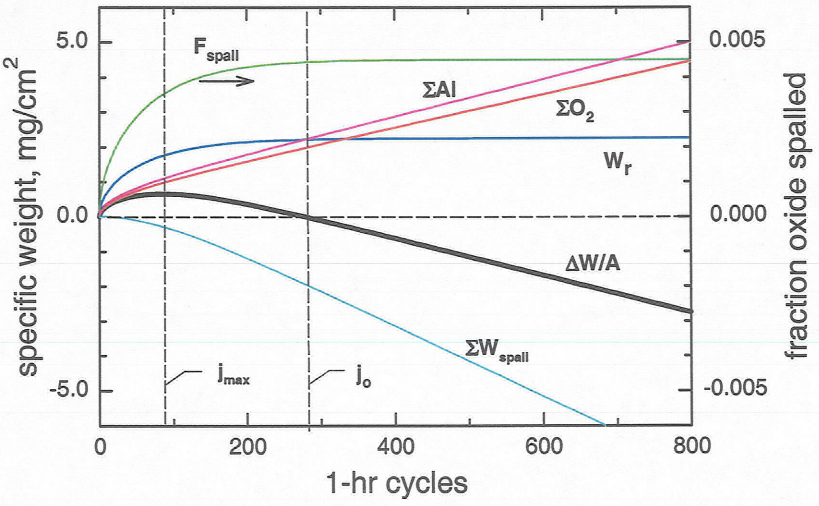

Figure 5. Various outputs of COSP cyclic oxidation model. Steady state behavior (i.e., limiting oxide thickness and linear rates of consumption and spalling) is achieved at ~ j_o. (Same model parameters as in Fig. 2 [2-4]).

DICOSM Equations and Characteristic Features

In order to demonstrate more explicit functional relationships between cyclic oxidation responses and the input parameters, some attention will now be given to the DICOSM model formulae. In the model derivation, the outputs have been expressed in terms of series summations involving the square root of an integer [5]:

$$\left(\frac{\Delta W}{A}\right)_A = F_A\sqrt{k_p\Delta t}\left\{(2-S_c)\sum_{i=1}^{j}\sqrt{i}+(n_o-j-1)\sqrt{j}\right\} \quad (5)$$

$$\left(\frac{\Delta W}{A}\right)_B = F_A\sqrt{k_p\Delta t}\left\{(2-S_c)\sum_{i=1}^{n_o}\sqrt{i}+[(1-S_c)(j-n_o)-1]\sqrt{n_o}\right\} \quad (6)$$

applying respectively to Case A, for cycle number $j \leq n_o$, and Case B, for cycle number $j \geq n_o$. Here n_o is the number of effective area segments, only one of which spalls per cycle, and is equivalent to the inverse of the area spall fraction, F_A. Accurate, closed form solutions have been obtained through the use of an algebraic substitution for the summation series, $\Sigma_j\sqrt{i} \cong \frac{1}{2}\, j^{1/2} + \frac{2}{3}\, j^{3/2}$, the Good-Smialek Approximation (GSA) [5].

The resulting algebraic expressions may be solved for $(\Delta W/A)_{max}$, j_{max}, j_o, and the terminal slope of mass loss, T.S [5]:

$$\left(\frac{\Delta W}{A}\right)_{GSA,max} \cong \frac{F_A\sqrt{k_p\Delta t}}{3}\left\{\frac{\left(\frac{2}{F_A}-S_c\right)^{3/2}}{(2(2S_c-1))^{1/2}}\right\} \quad (7)$$

$$J_{max} \cong \frac{\frac{2}{F_A}-S_c}{2(2S_c-1)} \quad (8)$$

$$J_{o,A} \cong \frac{3\left(\frac{2}{F_A} - S_c\right)}{2\,(2S_c - 1)} \qquad [9]$$

$$T.S. = -(S_c - 1)\sqrt{F_A k_p \Delta t} \qquad [10]$$

These relations explicitly define how key features (descriptive or characteristic parameters) vary directly with the model input variables. For example, it is easy to discern that the number of cycles to reach zero weight change, j_o, is exactly 3.0 times the number to reach maximum, j_{max}, and that each of these terms vary inversely with area spall fraction, F_A. The maximum in weight change varies with the square root of $k_p\Delta t$ and a more complex function of F_A and S_c. Finally the steady state rate of weight loss per cycle varies with S_c and the square root of the product of the spall fraction, growth rate, and cycle duration. Other attempts at expressions for characteristic parameters have been developed empirically and show some similarity to those above [1-7].

Universal (Normalized) DICOSM Cyclic Oxidation Behavior

Weight change curves. The simplicity of these DICOSM-GSA equations suggest some special constructions to describe general cyclic oxidation behavior. Dimensionsless, universal terms for weight change, W_u, and cycle number, J_u, are obtained by normalizing by corresponding $(\Delta W/A)_{max}$ and j_{max}, yielding the cyclic oxidation curve for Case A as [5,8,9]:

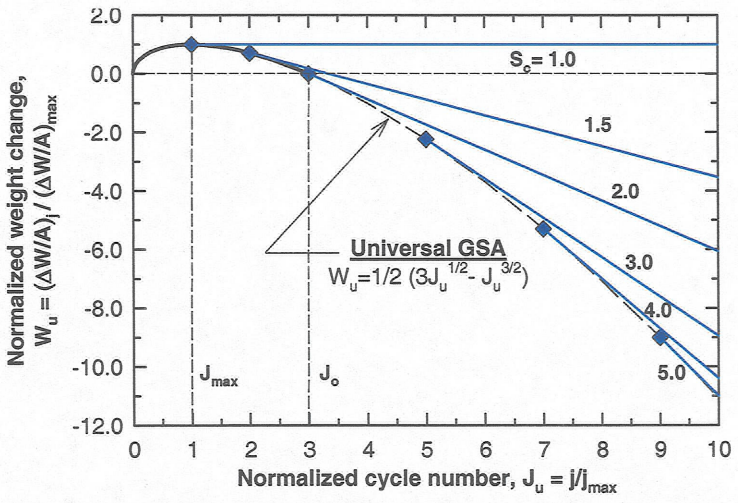

Figure 6. Universal DICOSM curves in which the weight change and cycle number are normalized by the coordinates at the maximum weight. A single curve is obtained for any k_p, Δt, or F_A for each S_c specified [9].

$$W_u = \frac{1}{2}\left[3J_u^{1/2} - J_u^{3/2}\right] \qquad (11)$$

This equation thus defines the universal cyclic oxidation weight change behavior for all values of the input parameters, up to the point where $j \geq n_o$, as shown in Fig. 6. Here the normalized weight change equals zero at the normalized cycle number of 3, and the maximum occurs at J_u= 1. The branches for the steady state portion, Case B, begin at $j = n_o$, which varies on the universal plot for differing oxides (shown here for S_c = 1 to 5). The steady state slopes must also vary (eqn. 10) and were verified empirically from running many combinations of input parameters.

Material consumed.

Now we consider the relations describing the amount of metal consumed, which is the pertinent quantity needed for failure criteria based on alloy depletion, mechanism changes, or breakaway oxidation [8,9]:

$$\Sigma W^{GSA}_{met,A} = (S_c - 1)F_A\sqrt{k_p\Delta t}\left\{n_o j^{1/2} + \frac{1}{3}j^{3/2}\right\}$$
$$\Sigma W^{GSA}_{met,B} = (S_c - 1)F_A\sqrt{k_p\Delta t}\left\{j n_o^{1/2} + \frac{1}{3}n_o^{3/2}\right\} \qquad (12A, B)$$

These equations may now be used to represent universal metal consumption for all DICOSM model parameters. The cycle number is normalized by the number of segments, n_o (=$1/F_A$), and the normalized weight change, $W_{met,u}$, is defined as eq. 13. The normalized metal consumption relations for Case A and B (eq. 14A, B) are produced, giving the single, continuous plot in Fig. 7:

$$W_{met,u} = \frac{\Sigma W_{met}}{\frac{4}{3}(S_c - 1)\sqrt{k_p \Delta t / F_A}} \qquad (13)$$

$$W_{met,u,A} = J_u^{1/2} + \frac{1}{3} J_u^{3/2}$$

$$W_{met,u,B} = J_u + \frac{1}{3} \qquad (14\ A, B)$$

In essence, this construction defines the amount of metal consumed for any combination of S_c, k_p, Δt, and F_A, with the transition to steady state behavior defined by the coordinates (1,1).

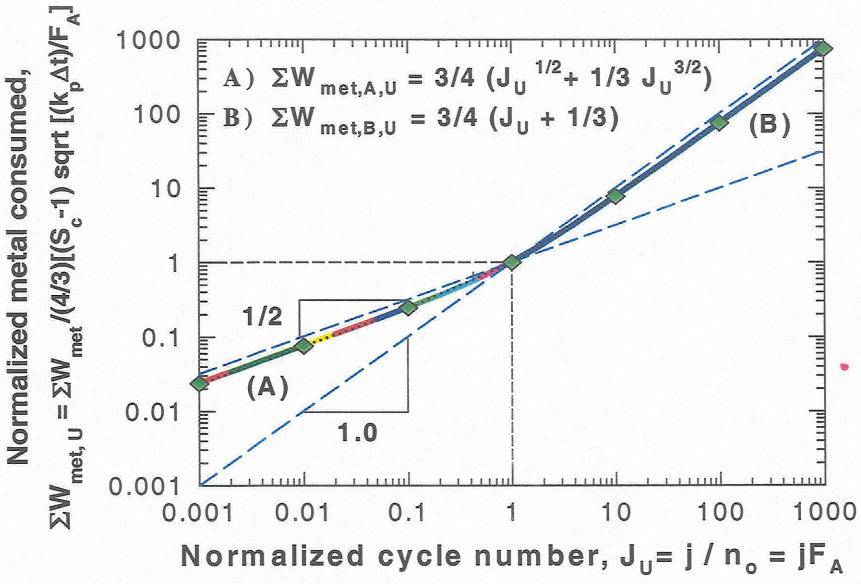

Figure 7. Universal, normalized curve for metal consumption. Universal transition point at the coordinates (1,1) and log-log slopes of 1/2 before and 1.0 after the transition [8,9].

Failure mapping. Finally, a universal construction has been applied to the concept of cyclic oxidation failure maps, modified from those first presented by Poquillion and Monceau [6,7]. Now a (critical) prescribed lifetime and prescribed amount of material consumed is presented on a spall constant, growth rate plot, or F_A-k_p diagram in the case of DICOSM. Again, by suitable normalization, a universal construction can be developed which defines the universal failure locus, once the specific failure criteria (j*, ΣW_m*) have been selected [9]. Four regimes or pseudo-quadrants of behavior are distinguished, corresponding to survival (I), or failure controlled by various combinations of spallation and scale growth (II,II,IV). By plotting published experimental data on such a map, for a failure criterion of 10 mg/cm^2 metal consumption in 1000 hr, it is seen that using the cyclic 1200°C oxidation data, $MoSi_2$ [10] and Zr-doped NiAl survive, whereas undoped NiAl fails primarily by spallation [11]. Similarly, the effect of sulfur on increased scale spallation had been plotted as a trend toward higher spall probabilities on a p–k_p map [7]. Finally, for a less demanding 100 hr life criterion, pure nickel is seen to fail by excessive growth at 1200°C [11] and pure copper fails at 500°C by contributions from both growth and spallation [12].

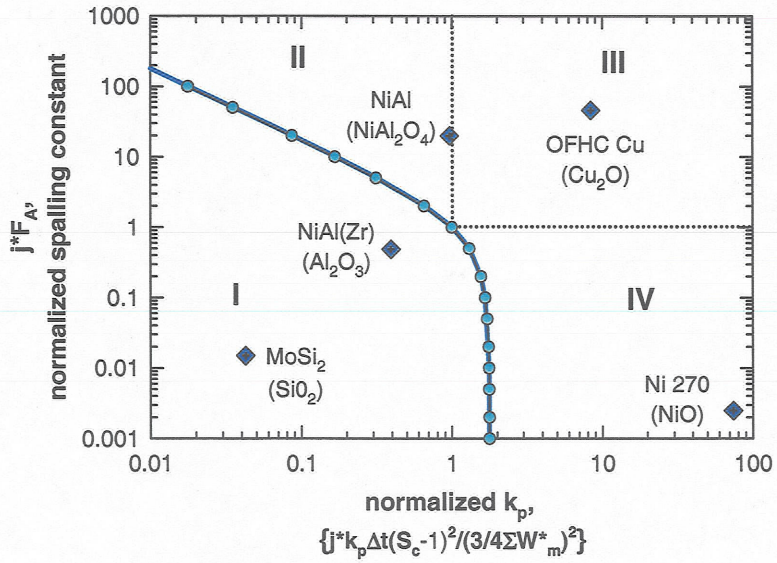

Figure 8. Universal F_A-k_p life map for DICOSM model, showing four major sectors and experimental results for diverse materials [9].

Survival appears as Region I, failure by spallation (II), growth (IV), or both (III).

Oxidative failure criteria set as 10 mg/cm^2 metal consumed in 1000 hr. for $MoSi_2$ and NiAl(±Zr) at 1200°C, in 100 hr for Ni at 1200°C;and in 100 hr for Cu at 500°C.

Concluding Remarks

This paper has reviewed the basic elements, assumptions, and outputs of cyclic oxidation models. Inherent in the COSP program is the flexibility to specify various scale growth kinetic laws, spall morphology, and thickness dependence. More severe material loss is seen to occur for interfacial spallation and when the spall fraction increases with scale thickness ($\alpha>0$). A special deterministic model (DICOSM) enabled simple mathematical approximations and normalization by performance terms. This allowed the construction of universal cyclic oxidation weight change, total metal consumption, and failure mapping plots for a wide variety of input parameters, indicating their generalized forms.

References

1. J.L. Smialek, *Metall. Trans.*, **9A**, pp. 309-320, (1978).
2. C.E. Lowell, C.A. Barrett, R.W. Palmer, J.V. Auping, and H.B. Probst, *Oxid. Met.*, **36**, pp.81-112, (1991).
3. J.L. Smialek, J.A. Nesbitt, C.A. Barrett, and C.E. Lowell: in *Cyclic Oxidation of High Temperature Materials*, M. Schutze and W.J. Quadakkers, eds., European Federation of Corrosion, Institute of Materials, London, pp. 148-168, (1999).
4. J.L. Smialek and J.V. Auping, Oxid. Met, **57**, pp. 559-581, (2002).
5. J.L. Smialek, *Acta materialia*, **51**, 2, pp. 469-483 (2003).
6. D. Poquillon and D. Monceau, *Oxid. Met.*, **59**, pp. 409-431, (2003).
7. D. Poquillon and D. Monceau, in *Materials Lifetime and Engineering Symposium*, P.K. Liaw et al., eds., TMS, Warrendale, PA, , pp. 165-172 (2003).
8. J.L. Smialek, ibid, pp.147-154.
9. J.L. Smialek, *Acta materialia*, accepted for publication, 2004.
10. M.G. Hebsur, M.V. Nathal. Strong, tough, and pest resistant $MoSi_2$–base hybrid composite for structural applications. NASA TM 107471, Washington, DC, Sept., 1997.
11. C.A. Barrett, A High Temperature Cyclic Oxidation Data Base for Selected Materials Tested at NASA Glenn Research Center. NASA TM 212546, Washington, DC, 2003.
12. L. T. Ogbuji, Oxidation resistance of advanced copper alloys. In *Corrosion science in the 21st century*, UMIST, Manchester, UK, July 6-11, 2003.